American Journal of Ophthalmology Case Reports 38 (2025) 102312

Contents lists available at ScienceDirect

American Journal of Ophthalmology Case Reports

journal homepage: www.ajocasereports.com/

Enhanced genotype-phenotype analysis using multimodal adaptive optics and 3D protein structure in Bietti Crystalline Dystrophy

Aarushi Kumar [a,b,f], Young Joo Sun [a,b,f], Ditte K. Rasmussen [a,b,c,f], Aubrey Hargrave [b], Claudia Phillips [a,b], Jennifer T. Vu [a,b], Mauricio G.S. Costa [d], Loh-Shan B. Leung [b], Charles Yu [b], Alfredo Dubra [b,*], Vinit B. Mahajan [a,b,e,**]

[a] Molecular Surgery Laboratory, Stanford University, Palo Alto, CA, USA
[b] Department of Ophthalmology, Byers Eye Institute, Stanford University, Palo Alto, CA, USA
[c] Department of Biomedicine, Aarhus University, Aarhus, Denmark
[d] Programa de Computação Científica, Vice-Presidência de Educação Informação e Comunicação, Fundação Oswaldo Cruz, Rio de Janeiro, Brazil
[e] Veterans Affairs Palo Alto Health Care System, Palo Alto, CA, USA

ARTICLE INFO

Keywords:
Retinal disease
Retinal dystrophy
Crystalline deposits
Genetic ocular disease
Adaptive optics
Bietti crystalline dystrophy
CYP4V2 protein

ABSTRACT

Purpose: Deep phenotyping of genetic retinal disease using multimodal adaptive optics ophthalmoscopy and protein structure variant analysis.

Observations: In a patient with extensive atrophy of the retinal pigment epithelium and yellow deposits in the retina, genetic testing identified two *CYP4V2* variants: c.802-8_810delinsGC and c.1169G > A, p.Arg390His. AI-generated protein structures indicated loss of CYP4V2 function. Reflectance confocal and multiple-scattering Adaptive Optics Scanning Light Ophthalmoscopy (AOSLO) captured crystalline deposits throughout the retina as well as previously unreported cyst-like structures that were mainly independent from the crystalline deposits. Sequential AOSLO imaging was conducted and revealed anatomical and morphological changes in the cysts and surrounding cellular structures.

Conclusions and importance: Cyst-like changes may represent a new BCD degenerative feature. Characterizing retinal genetic disease variants with protein structural modeling and phenotyping with AOSLO represents an advanced approach for clinical diagnosis and may serve as a biomarker of disease progression.

1. Introduction

Conventional characterization of genetic retinal disease involves statistical variant analysis and retinal imaging with fundus photography and Optical Coherence Tomography (OCT). Genotype-phenotype correlation is important because it allows the linking of a specific genetic mutation (genotype) to the observable characteristics of the disease in a patient (phenotype), which helps predict disease severity, progression, and potential treatment options. Genotype-phenotype correlation is also an essential basis for human retinal gene therapy trials. In many cases, however, standard genotyping and phenotyping are insufficient, especially in rare conditions like Bietti Crystalline Dystrophy (BCD). These patients display clinical characteristics commonly including yellow-white crystalline and/or complex lipid deposits along the retinal posterior pole and corneal limbus, atrophy of the retinal pigment epithelium (RPE), night blindness, and progressive vision loss.[1] These phenotypes typically appear in the second or third decade of life.[2] BCD affects one in every 67,000 people, although its prevalence varies throughout the world and is higher in European and East Asian populations.[2–4] It is a rare autosomal recessive retinal degeneration (OMIM #210370) associated with variants in the *CYP4V2* (cytochrome P450 family 4 subfamily V member 2) gene.[2,5] There are more than 100 identified disease-causing variants in *CYP4V2*, most of which are missense or large deletions.[2] Yet, similar to other genetic rare orphan eye diseases, *CYP4V2* genetic testing alone may not be sufficient to confirm BCD diagnosis (e.g., variants of unknown significance, penetrance, or compound heterozygosity), and may require additional validation. More recent technologies, such as artificial intelligence

* Corresponding author. Byers Eye Institute, Department of Ophthalmology, Stanford University, Palo Alto, CA, 94304, USA.
** Corresponding author. Byers Eye Institute, Department of Ophthalmology, Stanford University, Palo Alto, CA, 94304, USA.
E-mail addresses: adubra@stanford.edu (A. Dubra), vinit.mahajan@stanford.edu (V.B. Mahajan).
[f] Co-first authors.

https://doi.org/10.1016/j.ajoc.2025.102312
Received 11 September 2024; Received in revised form 6 March 2025; Accepted 17 March 2025
Available online 22 March 2025

(AI)-based protein structural modeling and deep phenotyping with adaptive optics (AO) could be integrated for a next-generation approach to characterize genetic retinal disease.

Molecularly, CYP4V2 is a family of omega-hydroxylases involved in breakdown of cellular lipids, and it is selective for mid-length fatty acid chains, particularly myristic acid [a saturated fatty acid (14:0); $CH_3(CH_2)_{12}COOH$].[6,7] A *CYP4V2* ortholog knockout mouse model displayed abnormal lipid metabolism and lipid crystal deposits in the mouse retina.[8] Therefore, the loss of CYP4V2 function may be directly involved in the formation of lipid deposits in BCD patients.[2,8–10] However, it is yet to be determined how BCD crystalline and lipid deposits are associated with cell death and damage, which might serve as important clinical biomarkers for BCD prognosis, progression, and future intervention.

Multimodal retinal imaging using adaptive optics scanning light ophthalmoscopy (AOSLO), optical coherence tomography (OCT), infrared (IR) fundus imaging, and color fundus imaging can be used to characterize retinal disease. The direct visualization of retinal structures at a microscopic scale *in vivo* provided by AOSLO represents a major addition to retinal imaging and could allow for early detection of genetic retinal disease.[11–13] The mosaic of photoreceptor outer segments can be observed directly on confocal reflectance AOSLO images,[14] with cone inner segments visible on split-X.[15] In addition, hyalocytes and some inner retinal pathologies such as microcysts have been visualized on split-X AOSLO.[16,17] It is especially valuable for studying retinal degeneration in which the outer segments are disrupted before the rest of the cell.[18]

2. Materials and methods

Study approval – The study adhered to the Tenets of the Declaration of Helsinki and Institutional Review Board (IRB)/Ethics Committee approval was obtained by Stanford University Institutional Review board. Informed consent was obtained from the patient.

Clinical imaging – Spectral domain optical coherence tomography (SD-OCT) and short-wavelength fundus autofluorescence (FAF) images were captured with a Spectralis (Heidelberg Engineering, Heidelberg, Germany).

Full-field electroretinography (ffERG) – ffERG was obtained with Dawson, Trick, and Litzkow (DTL)-recording electrodes and Ganzfield stimulation according to international standards as outlined by the International Society for Clinical Electrophysiology of Vision (ISCEV).[19]

Genetic sequencing and analysis – Sequence analysis was performed using the Blueprint Genetics My Retina Tracker panel [CLIA-certified (#99D2092375) laboratory]. Variants were identified using ClinVar and classified as "demonstrated links to ocular clinical phenotypes" if there are publications discussing the variant.

Pathogenicity prediction – *CYP4V2* missense variants and pathogenicity of amino acid substitutions were predicted and pathogenicity scores were acquired from AlphaMissense (https://console.cloud.google.com/storage/browser/dm_alphamissense).[20]

Structural modelling – The 3D structure of the CYP4V2 protein was predicted using AlphaFold (AlphaFold ID: AF-Q6ZWL3-F1).[21] The figure was generated using Pymol (The PyMOL Molecular Graphics System, Version 2.0 Schrödinger, LLC).

Adaptive optics imaging – The subjects' pupils were dilated using one drop of 1% tropicamide and one drop of 2.5% phenylephrine eye drops. Confocal and non-confocal split-X AOSLO image sequences of 150 frames were captured with 790 nm light, while focused in the inner retina and the photoreceptor layer at the foveal center. One or more minimally distorted images were selected from each sequence as a registration template. The template was used to register and average at least five images to create high signal-to-noise ratio images. The averaged images, each covering an area of about 1.5 degrees of visual angle, were manually tiled to cover the foveal avascular zone (Photoshop; Adobe Inc., San Jose, CA, USA).[22] Pathological structures such as cysts were manually traced on non-confocal split-detector images and binary masks of these areas were created using FIJI (ImageJ; National Institute of Health, Bethesda, MD): Cysts, n = 35; photoreceptors, n = 15. Feret's diameter (the distance between the two farthest points in the structure) were measured for each structure using MATLAB (MathWorks, Natick, MA, USA).

3. Results

Clinical findings – A 24-year-old male was referred for evaluation of nyctalopia that began five years prior. The patient had fatty liver disease but no other comorbidities. The extended family had no eye or liver disease. His visual acuity was 20/40 OD and 20/125 OS at baseline. Slit lamp examination demonstrated corneal deposits in both eyes without any signs of edema, atrophy, or scarring (Fig. 1A–E). Fundus examination revealed yellow refractile spots accumulated in the macula as well as the periphery of both eyes, while the disc and the vessels were normal (Fig. 1F–J). Short-wavelength fundus autofluorescence (FAF) seemed to be diminished suggesting RPE cell damage and loss (Fig. 1K–O). Optical coherence tomography (OCT) showed cystoid macular edema (CME) on the right eye, mild epiretinal membranes in both eyes, and loss of outer retinal lamination in both eyes (Fig. 1P–T). Full-field and multifocal electroretinogram (ffERG) demonstrated bilaterally symmetric diffuse dysfunction affecting both rod and cones (Fig. 1U–Z). Goldmann visual field (GVF) showed an enlarged blind spot and constriction of I4e to 30–40° on both eyes (Fig. 1AA-1AC). He was initially diagnosed with pigmentary retinal dystrophy and referred for genetic testing.

Genetics and structure-function analysis – Genetic testing revealed compound heterozygous variants for *CYP4V2* c.802-8_810delinsGC[23,24] and *CYP4V2* c.1169G > A, p.Arg390His,[25] which are both autosomal recessive pathogenic variants. Other variants identified were not expected to explain the patient's clinical presentation (**Supplemental Text**). Variant testing in the parents confirmed the variants occurred in *trans* (compound heterozygous): both his mother (*CYP4V2* c.802-8_810delinsGC, heterozygous) and father (*CYP4V2* c.1169G > A, heterozygous) were *CYP4V2*-variant carriers (Fig. 2A). We conducted a protein structure-function analysis based on an AI-generated three-dimensional (3D) CYP4V2 protein model structure (AlphaFold ID: AF-Q6ZWL3-F1) and AI algorithm testing of pathogenicity (AlphaMissense) to support the notion that the combination of these autosomal recessive patient variants would lead to the lack of CYP4V2 function (Fig. 2B).[20,21] CYP4V2 is a 525 amino acids-long peripheral membrane protein involved in fatty acid metabolism in the eye as well as other tissues (Fig. S1).[26] It consists of a transmembrane domain and a catalytic P450 domain which accommodates a heme-group to omega-hydroxylate polyunsaturated fatty acids (Fig. 2B).[27–29] The *CYP4V2* indel variant, c.802-8_810delinsGC, was at a canonical splice acceptor site of *CYP4V2* exon 7, which is subject to mRNA-decay resulting an absence of CYP4V2 protein or expected to result in a truncated CYP4V2 protein (p.Ser267fs*).[28] The potentially truncated CYP4V2 would be unlikely to fold into a proper P450 domain (Fig. 2C). Therefore, the *CYP4V2* c.802-8_810delinsGC variant is predicted to result in a non-functional CYP4V2 protein. The other pathogenic *CYP4V2* variant c.1169G > A resulted in an arginine to histidine mutation at residue 390 (p.Arg390His). In an AI-generated 3D protein structure, this arginine normally appears to be involved in multiple charge-charge and hydrogen bonding interactions at a hydrophilic packing interface (Fig. 2D). More specifically, the Arg390 neighbored heme-interacting residues such as Leu389 and Pro459 and the disruption of Arg390 by histidine likely affects the heme-dependent function of CYP4V2 (Fig. 2D). Similar molecular consequences are also observed in other pathogenic *CYP4V2* missense variants when mapped to this region, which strongly supports the potential molecular defects and pathology of p.Arg390His.[28,30] In parallel, we applied an AI-based protein structure-pathogenicity analysis of missense variants, AlphaMissense,[20] and this algorithm also predicted variants of the amino acid residues

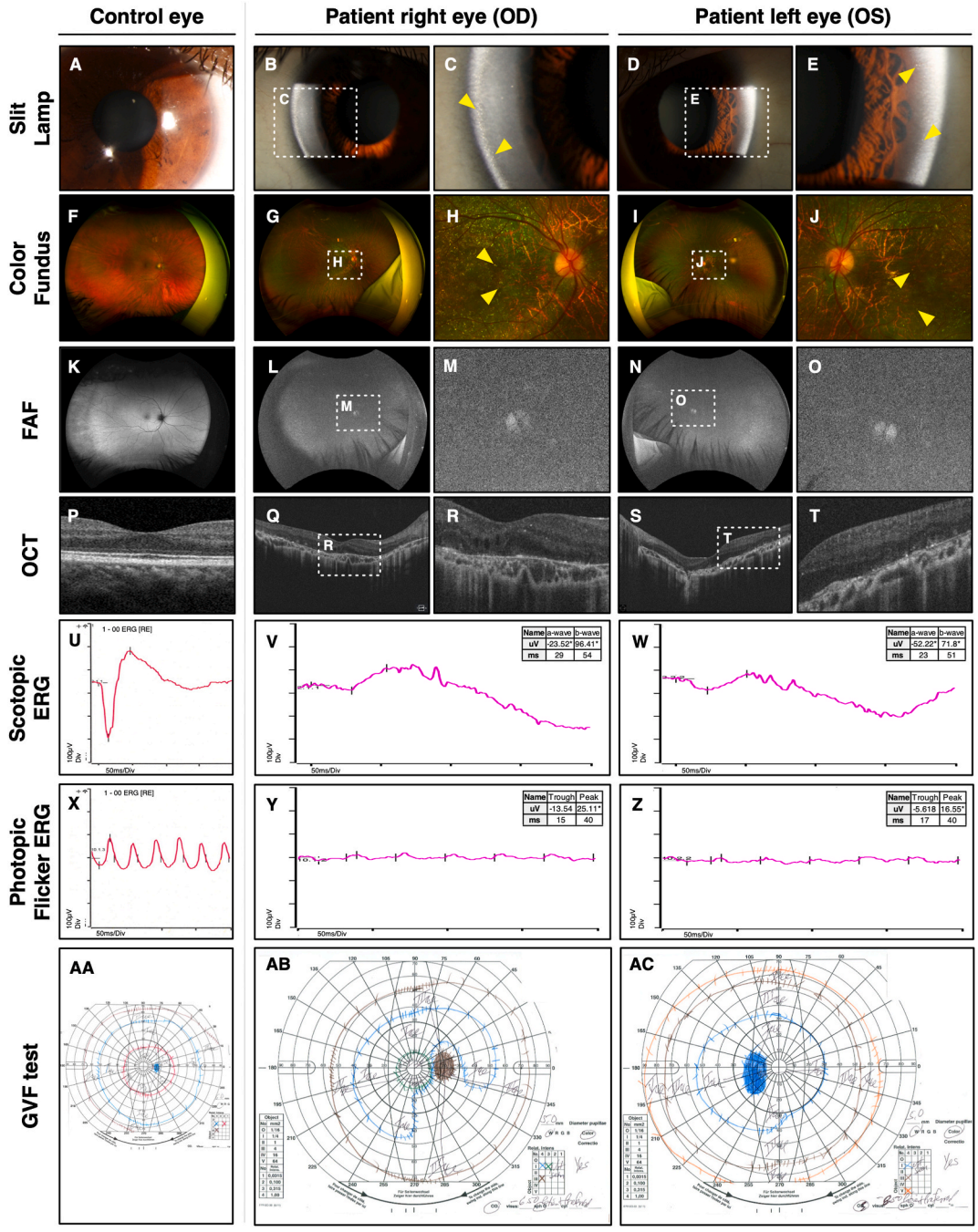

Fig. 1. Clinical examination: A-E) Slit lamp examination demonstrated corneal deposits and an otherwise normal anterior segment in both eyes. Yellow arrows indicate crystalline structures. **F-J)** Fundus examination revealed yellow refractile spots (yellow arrows) accumulated in the macula as well as the periphery of both eyes, and mild epiretinal membrane in both eyes. The disc and the vessels were normal. **K-O)** Fundus autofluorescence (FAF) was hazy suggesting a lack of natural fluorescence emitted by healthy retina. **P-T)** Optical coherence tomography (OCT) confirmed the Cystoid Macular Edema (CME) in the right eye along with mild epiretinal membrane and a loss of outer retinal layers in both eyes. **U-Z)** Full-field and multifocal electroretinogram (ffERG) demonstrated bilaterally symmetric diffuse retinal dysfunction affecting both rods and cones. **AA-AC)** Goldmann visual field (GVF) test suggested significant visual field defects with enlarged blind spots and I4e constricted to 30–40° in both eyes. I3e was perceived within a range of 10° in the right eye and not seen in the left eye. (For interpretation of the references to color in this figure legend, the reader is referred to the Web version of this article.)

neighboring the heme-interacting site, including 8 of each pathogenic variants and VUS, to be pathogenic (Fig. 2B). Combined with the patient's phenotypic presentation, these genetic and structure-function analyses strongly supported a diagnosis of Bietti Crystalline Dystrophy (BCD).

High resolution retinal imaging using AOSLO – Retinal regions of interest were identified by OCT and SLO IR imaging. OCT imaging revealed diffuse thinning of retinal layers (Fig. 3A–B). CME (Fig. 3C; purple arrows) and intraretinal crystalline structures (Fig. 3C; yellow arrows) mainly between the photoreceptor layer (PRL) and RPE, potentially with some crystals scattered diffusely throughout the inner retina. These crystals or hyper-reflective structures are absent in control subjects (Fig. 3D). The intensity patterns within the hyper-reflective features vary substantially, with some consisting of multi-speckled islands, and some on the nasal hemisphere forming a somewhat radial striation pattern (Fig. 3E–F). Since the vessels in our patient (Fig. 3E) are

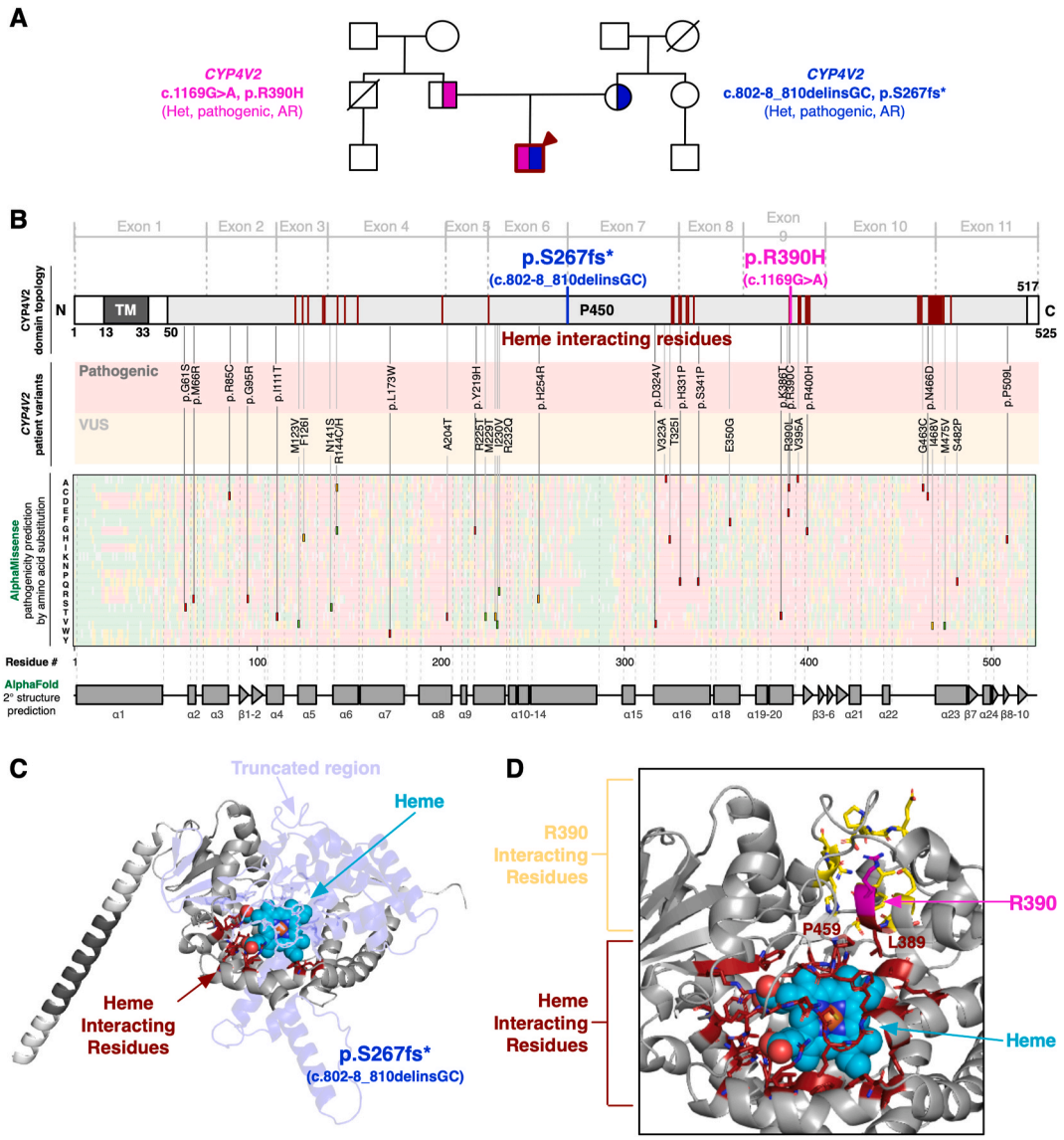

Fig. 2. Genetic and structure-pathology analysis: A) Index patient (dark red box with arrow) harbored compound heterozygous *CYP4V2* variants. c.1169G > A was inherited from his father (magenta) and c.802-9_810delinsGC was inherited from his mother (blue). Both parents are heterozygous and have no clinical phenotype. **B)** Protein domain topology map highlighting heme-interacting residues (dark red) as well as the patient's two *CYP4V2* variants (blue and magenta). Pathogenic *CYP4V2* missense variants (light red box) along with variants of unknown significance (VUS; light yellow box) near heme-interacting residues from ClinVar were mapped. Pathogenicity prediction by AI-tool (AlphaMissense) is shown as a heatmap: pathogenic (red), ambiguous (yellow), and benign (green). Predictions corresponding to each *CYP4V2* ClinVar variant were depicted as a box. Of 16 pathogenic variants, 15 were correctly predicted pathogenic and one was predicted as ambiguous by AlphaMissense. Secondary amino acid structure prediction was made by AlphaFold (α-helix: grey box, β-sheet: grey arrow). **C)** Structure-function analysis of *CYP4V2* variant c.802-9_810delinsGC showing potential truncation of the protein due to frameshift and premature stop-codon. **D)** *CYP4V2* variant c.1169G > A resulted in R390 mutation near the heme binding site. (For interpretation of the references to color in this figure legend, the reader is referred to the Web version of this article.)

darker than the ones in the control subject (Fig. 3D), the white regions in our patient cannot be RPE islands appearing white due to contrast differences but must truly be hyperreflective. Furthermore, some of these spots are located on top of blood vessels, indicating that they reside in the inner retina, in accordance with OCT volumetric imaging (Fig. 3B–C). Based on these findings, AOSLO imaging focused on the NFL and PRL (cyan and red, respectively, in Fig. 3B–C and **3E-F**) showed both CME and numerous crystalline structures that are absent in control eyes (Fig. 3G and 3J-O, Fig. S2), with the latter being 2–10 μm across, many of them oblong, and many of these oriented along the surrounding axon bundles, showing no obvious spatial correlation with adjacent blood vessels or capillaries (Fig. 3H–I) supporting the presence of crystalline deposits in the inner retina up to, and including, the NFL. AOSLO imaging also reveal few and sparse islands of photoreceptors (Fig. 3K–L), as opposed to the complete contiguous mosaic seen in the control subject (Fig. 3J), suggesting severe retina degeneration. Interestingly, the cyst-like circular and ovoidal structures in the non-confocal split-detection images (Fig. 3N–O, green arrows) did not align with the islands of hyperreflective spots seen on the corresponding confocal images (Fig. 3K–L, yellow arrows). Some of these putative cysts seem to have a smaller circular feature within them, akin to a cell nucleus (Fig. 3O, orange arrows and Fig. S3). Notably, the cyst-like structures near retinal vasculature outside of the foveal avascular zone (FAZ), were smaller, ranging from 1.8 to 14.3 μm in diameter, clustered and not related to the blood vessels.

Follow-up AOSLO imaging – Two years after the first (baseline) imaging, a follow-up imaging focused on the nominal photoreceptor layer, where the cyst-like structures were previously identified, was

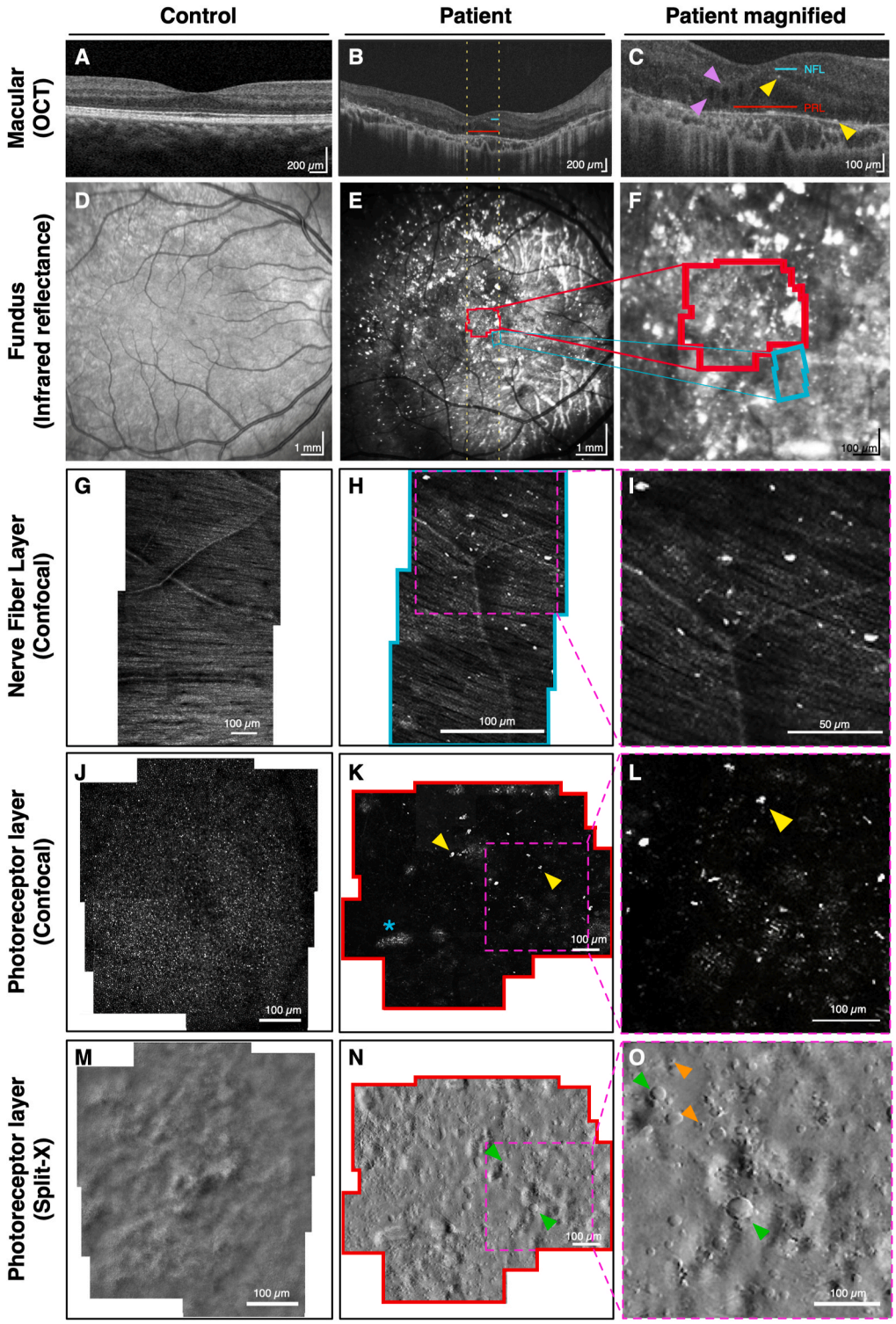

Fig. 3. Multimodal AOSLO imaging of index patient: A-C) Compared to a healthy control, our patient's OCT showcased diffuse thinning of layers and intraretinal crystalline structures. Cystoid macular edema (CME) (purple arrows) and crystals (yellow arrows) were not present in vessels, or the disc. Photoreceptor layer showed abnormalities. The approximate location of AO imaging was indicated as red (PRL) and cyan (NFL) lines. **D-F)** Infrared reflectance images guided the location of interest for AOSLO imaging. Compared to the control eye, the patient's eye displayed several hyperreflective areas. Imaged foveal photoreceptor layer is outlined in red and nerve fiber layer area is outlined in cyan. **G)** Confocal AOSLO imaging at the nerve fiber layer (NFL) showed well-organized nerve fibers (thin white lines) and blood vessels (thick white lines) in a healthy control, while **H-I)** crystalline structures (white spots) were present in our patient. **J-L)** Confocal AOSLO imaging confirmed an abnormal photoreceptor layer in our patient with an irregular cone mosaic and showed islands of hyperreflective spots (blue asterisk) along with hyperreflective crystalline structures (yellow arrows). The islands consisted of clusters of circular spots with hyperreflective signals similar to cone photoreceptors. **M-O)** AOSLO split-detector (Split-X) imaging at the photoreceptor layer revealed a novel feature: the presence of cyst-like structures that did not align with the hyperreflective photoreceptor islands seen on the confocal image (green arrows). Some of these structures harbored a central circular feature (orange arrows). (For interpretation of the references to color in this figure legend, the reader is referred to the Web version of this article.)

performed. Because of our insight gained from the first imaging session, we were able to focus on this specific area of interest. Islands of hyperreflective spots (Fig. 4A), and the novel cyst-like structures were observed again (Fig. 4B), some of them appear larger and with more irregular less defined edges. These larger cysts could not be identified by aligning with OCT images (Fig. 4A1). Furthermore, the smaller cysts appeared more uniform and circular (Fig. 4A2, 4B2), while there seemed to be a positive correlation between the size of the cysts (up to 104 μm in diameter) and the irregularity of their shapes. Taking account of the previously reported lensing effect of cysts in AOSLO images and the smoother edges in the Split-X images of the smaller cysts, these cysts are likely in the inner retina.[31] Sparse hyperreflective speckles of varying sizes were observed in the patient's confocal image (Fig. 4A3). This could be caused by cellular damage and distortion of photoreceptors due to the presence of crystalline structures between the photoreceptor and RPE layers. This notion is supported by the regular mosaic of features, which are most likely photoreceptor inner segments seen in non-confocal split-detection imaging (Fig. 4B3). Imaging of the nerve fibre layer recaptured the areas of hyperreflectivity representing crystalline structures (Fig. 4E). The absence of RPE cells in AOSLO dark field imaging further confirms that hyperreflectivity at the nominal (now atrophied) photoreceptor layer was not caused by islands of RPE[32] (Fig. 4G), when compared to the hexagonal mosaic seen in a control subject (Fig. 4H).

Follow-up clinical findings – At follow-up the patient's visual acuity was 20/50 OD and 20/300 OS. Fundus examination, FAF and OCT

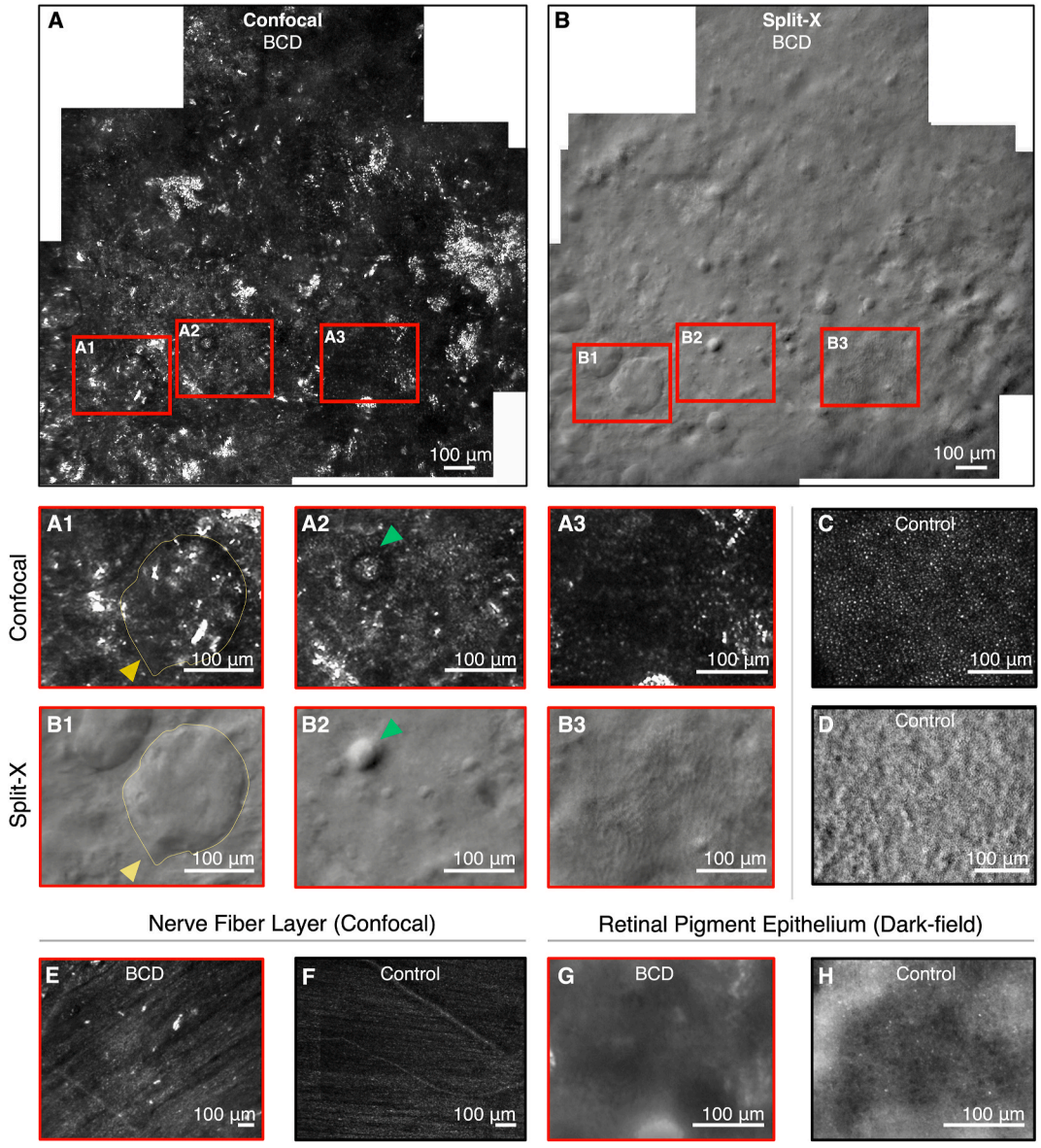

Fig. 4. Follow-up multimodal AOSLO imaging: A) Islands of hyperreflective spots were recaptured in the confocal AOSLO images of the patient's PRL. This time, cyst-like structures were also distinguishable unlike baseline imaging two years prior (**A1**; yellow arrow and **A2**; green arrow). Hyperreflective spots of varying sizes did not resemble a normal photoreceptor mosaic (**A3**). **B)** Cyst-like structures were also recaptured in the Split-X images. Larger pockets of fluid or cysts were evident on both confocal and Split-X imaging and had a more irregular boundary (**B1**; yellow area) compared to microcysts (**B2**; green arrow). A well demarcated microcyst appeared in both confocal and split-X imaging (green arrows). New features such as photoreceptor inner segments did not compare to the control image of rod cells and cone cells (**B3**). **C)** Confocal AOSLO image of healthy control PRL**. D)** Split-X AOSLO image of healthy control PRL. **E)** The areas of hyperreflectivity representing crystalline structures were recaptured in the confocal AOSLO image of the patient's NFL. **F)** Confocal AOSLO image of NFL of healthy control. **G)** Dark-field AOSLO image showcasing lack of cobblestone morphology of RPE layer. **H)** Dark-field AOSLO image of healthy control showing cobblestone morphology of RPE layer. (For interpretation of the references to color in this figure legend, the reader is referred to the Web version of this article.)

remained stable. They revealed yellow refractile spots, diffuse hypofluorescence indicating RPE cell damage or loss, and diffuse thinning with intraretinal crystals respectively.

4. Discussion

We presented a BCD patient with ocular imaging including reflectance and multiple scattering AOSLO, which allows phenotyping on a microscopic level for inherited retinal disease.[33] The patient underwent two consecutive AOSLO imaging sessions two years apart, capturing novel cyst-like structures in BCD, and hyper-reflective structures referred to as crystals in the literature, which confirmed the patient's diagnosis. These crystalline structures were mainly located within the FAZ with some present in the periphery, showing various intensity patterns within them. Although it was not possible to match specific features between imaging sessions, a general insight into the dynamic changes in BCD are captured.

Both patient variants are previously reported in literature, although not in the same patients. A case report of a 35-year-old lady with c.802-8_810delinsGC describes a mild phenotype with few crystalline deposits and almost normal vision.[23] A case series of variants including c.1169G > A, p.Arg390His describes a BCVA of 0.06/0.3,[25] which highlights the diverse phenotypes of BCD. In our case, protein structure-based *in silico* modelling of these variants added valuable insight into the molecular and functional consequence, in particular the missense c.1169G > A, p.Arg390His variant, which was revealed to disturb the heme-dependent function of CYP4V2 which could not be identified using conventional *in silico* analysis e.g. PolyPhen, SIFT.

The unusual appearance of the cone mosaic displaying only islands of waveguiding photoreceptors indicate damaged outer segments,[18] and clusters of surviving cone inner segments can be seen spread out in the periphery. These clusters correspond to hypo-reflective areas on the confocal and short-wavelength FAF images, indicating outer segment and RPE atrophy, respectively.

The smooth circular cyst-like structures found in AOSLO imaging are a previously unknown feature of BCD unrelated to the hyperreflective retinal areas. Follow-up multimodal AOSLO imaging provided clearer structural information on these cyst-like structures. They had uniform appearances with defined borders: the smooth circular nature of these structures suggests that they are more likely to be fluid-filled microcysts rather than solid crystals. The microcyst located within the FAZ were noticeably larger and more dispersed than the ones found outside, perhaps due to the absence of photoreceptors that would compete for space. Notably, as these cyst-like structures became bigger, they became more irregular in shape. It is hard to ascertain the role of cysts in the BCD pathology based on our current observations. Yet it is possible that these microcystic changes are an early feature of BCD and contribute to the later degeneration of the photoreceptors. While larger macular cysts are well-described in BCD patients[34] and also present in degenerative diseases like Best Vitelliform Macular Dystrophy,[35] this is to our knowledge the first description of these microcysts in BCD. Longitudinal follow up or endeavors to identify this feature in a large cohort of early stage BCD patients will be valuable. The smaller cysts (Fig. 4A2, 4B2) showed a near identical shape to the ones found in a commotio retinae—traumatic retinopathy secondary to direct or indirect trauma to the globe—patient,[31] where AOSLO imaging revealed a microcyst that could not be seen on OCT, as in our case as well. The size of the microcysts that we picked up are down to 1.8 μm, which is below the resolution of standard OCT images which is 10–15 μm. Therefore, it is impossible to identify our cysts in standard OCT imaging. Furthermore, side-by-side comparison of traditional retinal imaging with structures identified by AOSLO proved difficult due to poor fixation and lack of landmarks such as blood vessels over the imaged areas. The larger cysts (Fig. 4A1, 4B1) were comparable to those of Best vitelliform macular dystrophy (also known as Best disease)[35] or macular hole patients.[36] Histopathological examination of these cysts may provide further insights on their molecular characteristics and origin.

The smaller scattered hyperreflective spots could be mistaken for rod photoreceptors, but more closely resemble remnants of cone photoreceptors with irregular appearance and larger dimensions. Nonetheless, if these were indicative of abnormal photoreceptor cells, the patient's vision would be poorer than the 20/50 recorded for the subject. This could be explained by misalignment of the photoreceptors which may not be seen in AOSLO confocal images if they are pointing away from the pupil center. The presence of crystals between the RPE and photoreceptor layer could cause such a change in photoreceptor orientation. Therefore, although it can be seen in both OCT and AOSLO imaging that the photoreceptor layer is not intact, this could be the result of a mix of photoreceptor damage and misalignment.

Non-confocal split-detector imaging can be a valuable tool for the study of retinal dystrophies, such as BCD,[37] which affect the outer cone segments before the remainder of the cell.[18] There have been many advances in gene augmentation studies for BCD,[38,39] along with ongoing AAV-vector-mediated gene replacement therapy trials (phase 1: NCT04722107 and NCT05694598) that aim to restore dysfunctional photoreceptors. Split-detector AOSLO imaging could be utilized to gather information about the extent of photoreceptor preservation to predict the level of achievable visual recovery based on anatomical factors ahead of gene therapy interventions.[15,40] Furthermore, understanding the extent of the remaining cone structure could contribute to assessing the actual benefit that the intervention could provide for each participant.[15]

Although deep phenotyping with AOSLO imaging presented in this study provides valuable insight into the pathology of Bietti Crystalline Dystrophy, our study has limitations. Mainly, our observations are based on a single patient, which limits the generalizability of our findings. Yet, these findings are in line with the current knowledge on BCD obtained in reports of other cases, and therefore likely representative of the phenotype. Another limitation may be in the interpretation of which retinal structure causes the appearance of the hyperreflective areas and cysts seen in our imaging. Although our interpretations are based on existing literature on AO-imaging in BCD, they may allow subjectivity by individual investigators. Therefore, all images have been interpreted independently by multiple investigators before conclusions were drawn. The imaging technique itself also presents challenges, including the fact that the instrument is optimized to visualize photoreceptor cells that are pointing directly towards the pupil, which we have considered in our interpretation. Furthermore, while our sequential imaging provides more insight into the time-dependent changes in the retina of our patient, we were unable to match any features from the baseline to the follow-up images despite having imaged the same area of the retina. This suggests either the topography of the retina changed drastically after two years, or the locus of fixation has moved. However, they allowed insight into the presence of crystals and cysts over time.

5. Conclusions

Here, we demonstrate how contextual *in silico* protein structure-function analysis strengthens the genetic diagnosis of BCD, and comprehensive, longitudinal clinical phenotyping and imaging from organ to cell level (deep phenotyping) identified progressive features of BCD.

CRediT authorship contribution statement

Aarushi Kumar: Writing – review & editing, Writing – original draft, Visualization, Methodology, Investigation, Formal analysis, Data curation. **Young Joo Sun:** Writing – review & editing, Writing – original draft, Visualization, Project administration, Methodology, Investigation, Formal analysis, Data curation, Conceptualization. **Ditte K. Rasmussen:** Writing – review & editing, Writing – original draft, Visualization, Methodology, Investigation, Formal analysis, Data curation. **Aubrey**

Hargrave: Writing – review & editing, Formal analysis, Data curation. **Claudia Phillips:** Writing – review & editing, Writing – original draft, Data curation. **Jennifer T. Vu:** Writing – review & editing, Writing – original draft, Data curation. **Mauricio G.S. Costa:** Writing – review & editing, Data curation. **Loh-Shan B. Leung:** Writing – review & editing, Resources, Formal analysis, Data curation. **Charles Yu:** Writing – review & editing, Resources, Formal analysis, Data curation. **Alfredo Dubra:** Writing – review & editing, Supervision, Project administration, Funding acquisition, Conceptualization. **Vinit B. Mahajan:** Writing – review & editing, Supervision, Project administration, Funding acquisition, Conceptualization.

Patient consent to publication

The patient provided written informed consent.

Institutional Review Board statement

The study was approved by the Stanford University Institutional Review Board and adhered to the tenets set forth in the Declaration of Helsinki.

Financial Support

VBM and AD are supported by (R01EY031360 and P30EY026877) and the Research to Prevent Blindness, New York, New York. VBM is also supported by NIH grants (R01EY031952 and R01EY030151) and the Stanford Center for Optic Disc Drusen. AD is also supported by NIH grants (R01EY032147 and R01EY032669). YJS is supported by Bright-Focus Foundation's Macular Degeneration Research program. DKR is supported by the DARE Fellowship, which is sponsored by the Lundbeck Foundation, and the VitreoRetinal Surgery Foundation Fellowship. Role of the Sponsor: The funding organizations had no role in design and conduct of the study; collection, management, analysis, and interpretation of the data; preparation, review, or approval of the manuscript; and decision to submit the manuscript for publication.

Declaration of competing interest

The authors declare that they have no known competing financial interests or personal relationships that could have appeared to influence the work reported in this paper.

Appendix A. Supplementary data

Supplementary data to this article can be found online at https://doi.org/10.1016/j.ajoc.2025.102312.

References

1. Halford S, Liew G, Mackay DS, et al. Detailed phenotypic and genotypic characterization of bietti crystalline dystrophy. *Ophthalmology*. 2014;121(6):1174–1184. https://doi.org/10.1016/j.ophtha.2013.11.042.
2. Garcia-Garcia GP, Martinez-Rubio M, Moya-Moya MA, Perez-Santonja JJ, Escribano J. Current perspectives in Bietti crystalline dystrophy. *Clin Ophthalmol*. 2019;13:1379–1399. https://doi.org/10.2147/OPTH.S185744.
3. Jiao X., Munier F.L., Iwata F., et al. Genetic linkage of Bietti crystallin corneoretinal dystrophy to chromosome 4q35. *Am J Hum Genet. Nov*. 2000;67(5):1309–1313. https://doi.org/10.1016/S0002-9297(07)62960-7.
4. Jiao X, Li A. Jin Z.B., et al. Identification and population history of CYP4V2 mutations in patients with Bietti crystalline corneoretinal dystrophy. *Eur J Hum Genet. Apr*. 2017;25(4):461–471. https://doi.org/10.1038/ejhg.2016.184.
5. Bietti G. Ueber faxmiliares Vorkommen von "Retinitis punctata albescens" (verbunden mit "dystrophis marginalis cristallinea cornea"), glitzern, des glaskorpers und anderen degenerativen augenveranderungen. *Klin Monbl Augenkeilkd*. 1937;99:737–759.
6. Hsu MH, Savas U, Griffin KJ, Johnson EF. Human cytochrome p450 family 4 enzymes: function, genetic variation and regulation. *Drug Metab Rev*. 2007;39(2-3):515–538. https://doi.org/10.1080/03602530701468573.
7. Nakano M, Kelly EJ, Rettie AE. Expression and characterization of CYP4V2 as a fatty acid omega-hydroxylase. *Drug Metab Dispos*. Nov 2009;37(11):2119–2122. https://doi.org/10.1124/dmd.109.028530.
8. Wang Y, Liu Y, Liu S, et al. A novel and efficient murine model of Bietti crystalline dystrophy. *Dis Model Mech*. 2022;15(3). https://doi.org/10.1242/dmm.049222.
9. Jiang JL, Qian FJ, Xiao DH, et al. Relationship of familial cytochrome P450 4V2 gene mutation with liver cirrhosis: a case report and review of the literature. *World J Clin Cases*. 2022;10(28):10346–10357. https://doi.org/10.12998/wjcc.v10.i28.10346.
10. Meng XH, He Y, Zhao TT, Li SY, Liu Y, Yin ZQ. Novel mutations in CYP4V2 in Bietti corneoretinal crystalline dystrophy: next-generation sequencing technology and genotype-phenotype correlations. *Mol Vis*. 2019;25:654–662 [Online]. Available: https://www.ncbi.nlm.nih.gov/pubmed/31741654.
11. Lombardo M, Serrao S, Devaney N, Parravano M, Lombardo G. Adaptive optics technology for high-resolution retinal imaging. *Sensors (Basel)*. Dec 27 2012;13(1):334–366. https://doi.org/10.3390/s130100334.
12. Gocho K, Kameya S, Akeo K, et al. High-resolution imaging of patients with bietti crystalline dystrophy with CYP4V2 mutation. *J Ophthalmol*. 2014;2014:283603. https://doi.org/10.1155/2014/283603.
13. Wang W, Chen W, Bai X, Chen L. Multimodal imaging features and genetic findings in Bietti crystalline dystrophy. *BMC Ophthalmol*. Aug 15 2020;20(1):331. https://doi.org/10.1186/s12886-020-01545-3.
14. Dubra A, Sulai Y, Norris JL, et al. Noninvasive imaging of the human rod photoreceptor mosaic using a confocal adaptive optics scanning ophthalmoscope. *Biomed Opt Express*. 2011;2(7):1864–1876. https://doi.org/10.1364/BOE.2.001864.
15. Scoles D, Sulai YN, Langlo CS, et al. In vivo imaging of human cone photoreceptor inner segments. *Investig Ophthalmol Vis Sci*. 2014;55(7):4244–4251. https://doi.org/10.1167/iovs.14-14542.
16. Migacz JV, Otero-Marquez O, Zhou R, et al. Imaging of vitreous cortex hyalocyte dynamics using non-confocal quadrant-detection adaptive optics scanning light ophthalmoscopy in human subjects. *Biomed Opt Express*. 2022;13(3):1755–1773. https://doi.org/10.1364/boe.449417 (in eng).
17. Beykin G, Norcia AM, Srinivasan VJ, Dubra A, Goldberg JL. Discovery and clinical translation of novel glaucoma biomarkers. *Prog Retin Eye Res*. Jan 2021;80, 100875. https://doi.org/10.1016/j.preteyeres.2020.100875 (in eng).
18. Litts KM, Cooper RF, Duncan JL, Carroll J. Photoreceptor-based biomarkers in AOSLO retinal imaging. *Investig Ophthalmol Vis Sci*. May 1 2017;58(6):BIO255–BIO267. https://doi.org/10.1167/iovs.17-21868.
19. McCulloch DL, Marmor MF, Brigell MG, et al. ISCEV Standard for full-field clinical electroretinography (2015 update). *Doc Ophthalmol. Feb*. 2015;130(1):1–12. https://doi.org/10.1007/s10633-014-9473-7.
20. Cheng J, Novati G, Pan J, et al. Accurate proteome-wide missense variant effect prediction with AlphaMissense. *Science*. 2023;381(6664):eadg7492. https://doi.org/10.1126/science.adg7492.
21. Jumper J, Evans R, Pritzel A, et al. Highly accurate protein structure prediction with AlphaFold. *Nature*. 2021;596(7873):583–589. https://doi.org/10.1038/s41586-021-03819-2.
22. Hargrave A, Sredar N, Khushzad J, et al. Novel foveal features associated with vision impairment in multiple sclerosis. *Investig Ophthalmol Vis Sci*. 2021;62(12):27. https://doi.org/10.1167/iovs.62.12.27.
23. Wang T, Chen Q, Yao X, et al. New compound heterozygous CYP4V2 mutations in bietti crystalline corneoretinal dystrophy. *Gene*. 2021;790:145698. https://doi.org/10.1016/j.gene.2021.145698 (in eng).
24. Murakami Y, Koyanagi Y, Fukushima M, et al. Genotype and long-term clinical course of bietti crystalline dystrophy in Korean and Japanese patients. *Ophthalmol Retina*. 2021;5(12):1269–1279. https://doi.org/10.1016/j.oret.2021.02.009 (in eng).
25. Xiao X, Mai G, Li S, Guo X, Zhang Q. Identification of CYP4V2 mutation in 21 families and overview of mutation spectrum in Bietti crystalline corneoretinal dystrophy. *Biochem Biophys Res Commun*. Jun 3 2011;409(2):181–186. https://doi.org/10.1016/j.bbrc.2011.04.112.
26. Karlsson M, Zhang C, Méar L, et al. A single-cell type transcriptomics map of human tissues. *Sci Adv*. 2021;7(31). https://doi.org/10.1126/sciadv.abh2169 (in eng).
27. Shan M, Dong B, Zhao X, et al. Novel mutations in the CYP4V2 gene associated with Bietti crystalline corneoretinal dystrophy. *Mol Vis*. 2005;11:738–743 [Online]. Available: https://www.ncbi.nlm.nih.gov/pubmed/16179904.
28. Li A, Jiao X, Munier FL, et al. Bietti crystalline corneoretinal dystrophy is caused by mutations in the novel gene CYP4V2. *Am J Hum Genet. May*. 2004;74(5):817–826. https://doi.org/10.1086/383228.
29. Kumar S. Comparative modeling and molecular docking of orphan human CYP4V2 protein with fatty acid substrates: insights into substrate specificity. *Bioinformation*. 2011;7(7):360–365. https://doi.org/10.6026/97320630007360.
30. Lockhart CM, Smith TB, Yang P, et al. Longitudinal characterisation of function and structure of Bietti crystalline dystrophy: report on a novel homozygous mutation in CYP4V2. *Br J Ophthalmol. Feb*. 2018;102(2):187–194. https://doi.org/10.1136/bjophthalmol-2016-309696.
31. Langlo CS, Flatter JA, Dubra A, Wirostko WJ, Carroll J. A lensing effect of inner retinal cysts on images of the photoreceptor mosaic. *Retina*. Feb 2014;34(2):421–422. https://doi.org/10.1097/IAE.0b013e3182a2f50c.
32. Scoles D, Sulai YN, Dubra A. In vivo dark-field imaging of the retinal pigment epithelium cell mosaic. *Biomed Opt Express*. 2013;4(9):1710–1723. https://doi.org/10.1364/boe.4.001710 (in eng).
33. Georgiou M, Litts KM, Kalitzeos A, et al. Adaptive optics retinal imaging in CNGA3-associated achromatopsia: retinal characterization, interocular symmetry, and intrafamilial variability. *Investig Ophthalmol Vis Sci*. 2019;60(1):383–396. https://doi.org/10.1167/iovs.18-25880.

34. Saatci AO, Doruk HC, Yaman A. Cystoid macular edema in bietti's crystalline retinopathy. *Case Rep Ophthalmol Med*. 2014;2014:964892. https://doi.org/10.1155/2014/964892.
35. Scoles D, Sulai YN, Cooper RF, et al. Photoreceptor inner segment morphology in best vitelliform macular dystrophy. Retina. *Apr*. 2017;37(4):741–748. https://doi.org/10.1097/IAE.0000000000001203.
36. Randerson EL, Davis DB, Higgins BP, et al. Assessing photoreceptor structure in macular hole using split-detector adaptive optics scanning light ophthalmoscopy. *Eur Ophthalmic Rev*. 2015;9:59.
37. Dolz-Marco R, Litts KM, Tan ACS, Freund KB, Curcio CA. The evolution of outer retinal tubulation, a neurodegeneration and gliosis prominent in macular diseases. *Ophthalmology*. Sep 2017;124(9):1353–1367. https://doi.org/10.1016/j.ophtha.2017.03.043.
38. Wang JH, Lidgerwood GE, Daniszewski M, et al. AAV2-mediated gene therapy for Bietti crystalline dystrophy provides functional CYP4V2 in multiple relevant cell models. *Sci Rep*. 2022;12(1):9525. https://doi.org/10.1038/s41598-022-12210-8.
39. Qu B, Wu S, Jiao G, et al. Treating Bietti crystalline dystrophy in a high-fat diet-exacerbated murine model using gene therapy. *Gene Ther*. 2020;27(7–8):370–382. https://doi.org/10.1038/s41434-020-0159-3.
40. Thomas MG, McLean RJ, Kohl S, Sheth V, Gottlob I. Early signs of longitudinal progressive cone photoreceptor degeneration in achromatopsia. *Br J Ophthalmol*. Sep 2012;96(9):1232–1236. https://doi.org/10.1136/bjophthalmol-2012-301737.